Calicivirus VP2 forms a portal-like assembly following receptor engagement.

Michaela J. Conley[1], Marion McElwee[1], Liyana Azmi[2], Mads Gabrielsen[3], Olwyn Byron[4], Ian G. Goodfellow[5] and David Bhella[1*]

[1] Medical Research Council – University of Glasgow Centre for Virus Research, Sir Michael Stoker Building, Garscube Campus, 464 Bearsden Road, Glasgow G61 1QH, United Kingdom

[2] Institute of Infection, Immunity and Inflammation, University of Glasgow, Sir Graeme Davies Building, 120 University Place, Glasgow, G12 8TA, United Kingdom

[3] CRUK Beatson Institute, Garscube Campus, Switchback Road, Glasgow, G61 1BD, United Kingdom

[4] School of Life Sciences, University of Glasgow, Sir Graeme Davies Building, 120 University Place, Glasgow G12 8TA, United Kingdom

[5] Division of Virology, Department of Pathology, University of Cambridge, Addenbrooke's Hospital, Hills Road, Cambridge CB2 2QQ, United Kingdom

***Corresponding Author**

Email david.bhella@glasgow.ac.uk

Tel +44 (0)141 330 3685

Fax +44 (0)141 337 2236

Abstract

To initiate infection many viruses enter their host cells by triggering endocytosis following receptor engagement. The mechanisms by which non-enveloped viruses escape the endosome are however poorly understood. Here we present near-atomic resolution cryoEM structures for feline calicivirus (FCV) both undecorated and labelled with a soluble fragment of its cellular receptor feline junctional adhesion molecule A (fJAM-A). We show that VP2, a minor capsid protein encoded by all caliciviruses [1,2], forms a large portal-like assembly at a unique three-fold symmetry axis following receptor engagement. This feature, which was not detected in undecorated virions, is formed of twelve copies of VP2 arranged with their hydrophobic N-termini pointing away from the virion surface. Local rearrangement at the portal site leads to opening of a pore in the capsid shell. We hypothesise that the portal-like assembly functions as a channel for delivery of the calicivirus genome through the endosomal membrane into the cytoplasm of a host cell to initiate infection. While VP2 was known to be critical for the production of infectious virus [3], its structure and function were hitherto undetermined. Our findings therefore represent a major step forward in our understanding of the *Caliciviridae*.

Main Text

The *Caliciviridae* family of viruses includes noroviruses and sapoviruses, which cause outbreaks of acute gastroenteritis in humans known as winter vomiting disease [4,5]. Feline calicivirus (FCV), a major cause of respiratory disease in felids [6], represents an excellent model system for the study of calicivirus biology as it is readily propagated *in vitro* and is one of only three caliciviruses to date for which a protein receptor has been identified [7].

Caliciviruses have small positive sense RNA genomes (~7.5 kb) that are packaged within a T=3 icosahedral shell, assembled from 180 copies of the major capsid protein (VP1) in three quasi-equivalent settings. Termed A, B and C, these VP1 conformers form 90 dimeric capsomeres. AB capsomeres are arranged around the 5-fold symmetry axes while CC capsomeres are located at the 2-fold symmetry axes [8]. The mature capsid protein has a short N-terminal arm (NTA), a shell (S) domain, comprising an eight-stranded antiparallel β-barrel motif, and a protruding (P) domain. The P domain is divided into the proximal P1 and distal P2 sub-domains, with P2 incorporating the receptor binding site and major immunodominant epitopes. In addition to VP1, an essential minor capsid protein VP2 is also incorporated into the virion at low copy number [1-3].

To initiate infection, FCV binds to the tight-junction cell-adhesion molecule feline junctional adhesion molecule-A (fJAM-A) [7]. JAM-A comprises a short cytoplasmic tail, a transmembrane domain and two immunoglobulin-like domains (D1 and D2). X-ray crystallography studies of murine and human JAM-A have shown them to form U-shaped homodimers via interactions at the membrane distal D1 [9,10]. We have previously shown that the outer face of FCV P2 binds to fJAM-A D1 causing the capsid spikes to rotate

63 approximately 15° counter-clockwise [11,12]. We hypothesised that these conformational
64 changes were priming events that would prepare the virion for genome release following
65 internalisation. FCV enters cells via clathrin-mediated endocytosis. Endosomal acidification
66 has been shown to be a necessary step in the viral entry process, although the mechanisms
67 by which the virus escapes the endosome have not been elucidated [13].
68
69 To construct an atomic resolution model of FCV interacting with its cellular receptor fJAM-A
70 and resolve the molecular detail of conformation changes induced, we collected high-
71 resolution cryo-EM images of FCV, both decorated with fJAM-A and undecorated. These
72 data were processed to calculate icosahedral reconstructions of unlabelled and receptor
73 bound virions at resolutions of 3 and 3.5 Å respectively (fig. 1a,b, ED 1, Supplemental Video
74 1). Blurring of the P-domain and receptor density in the FCV-fJAM-A map confirmed our
75 previous findings that conformational changes following receptor engagement break
76 icosahedral symmetry and result in incoherent averaging [11,12]. To address this, we first
77 performed model-based classification of FCV-fJAM-A in pre and post-conformational change
78 states [12]. We identified a very small subset of particles that were found to be in a pre-
79 conformational change state, i.e. all of the capsomeres were in the same orientation as the
80 undecorated virus (ED2). The vast majority of particles however were grouped into classes
81 in which the P-domains remained poorly resolved, indicating that the receptor induced
82 conformational change is not coordinated. To calculate 3D reconstructions at sufficiently
83 high resolution to allow building of atomic models of FCV P-dimers bound to fJAM-A, we
84 adopted a focussed classification approach [14-16]. This yielded 3D reconstructions of
85 individual capsomeres with improved resolution, revealing the range and extent of
86 conformational changes in both AB and CC dimers (ED2, Supplemental Video 2).

In the course of this analysis three classes emerged in which we saw a previously unreported structure. Twelve fingers of density protrude from the capsid floor, arranged about a three-fold symmetry axis (ED 2, Supplemental Video 2). The P-fJAM-A density in these classes was determined at improved resolution, suggesting that the capsomeres were constrained by the presence of the novel feature. A second focussed classification experiment was performed at the three-fold axis confirming the presence of a large dodecameric portal-like assembly extending approximately 13 nm from the capsid shell (fig. 1c-e, ED 3, Supplemental Video 3). The predominantly alpha-helical protein monomers are arranged in a circle about the icosahedral three-fold symmetry axis, forming a funnel-shaped structure that is 7nm in diameter at its base and 5nm in diameter at its tip, where the density becomes fuzzy and poorly resolved. There is an opening in the capsid shell at the portal-associated three-fold symmetry axis that is not seen at non-portal axes (fig. 1d, ED 3d, Supplemental Video 3). Our analysis shows that the most populous class of virions present a single portal at a unique three-fold axis (ED 3e).

To test whether the portal-like structure was present in undecorated particles, we performed the same focussed-classification analysis on our undecorated dataset. No such feature was found, indicating that the assembly emerges from within the virion following receptor engagement. An analogous structure has been described for the single stranded DNA containing bacteriophage ΦX174 [17]. This virus encodes a protein (H) that assembles a tube at a unique 5-fold axis following host engagement. The 'H-tube' penetrates the bacterial cell wall to deliver the viral genome.

Our atomic model of VP1 for the FCV vaccine strain F9 closely matches that of the virulent systemic (VS) FCV strain 5 [18], with the most significant differences being in the P2 domain (ED 4 and 5, Supplemental Video 4). Within this region we saw density consistent with the presence of a metal ion. This has not been reported in any calicivirus VP1 structures to date and was strongly resolved with density visible at an isosurface threshold 12 σ above the mean intensity. The distances between the putative metal-ion density and surrounding oxygens (~2.8 Å), along with the preponderance of main-chain carbonyl interactions, lead us to suggest that potassium is the most likely candidate for these densities [19]. Mutational analysis and sequence comparisons of VS-FCV and non-VS strains suggest that the metal-binding site may be important for infectivity and pathogenesis [20] (ED 4).

Atomic models for FCV VP1, VP2 and fJAM-A were built into the asymmetric FCV-fJAM-A density map at the C3 portal-vertex (ED 5). The asymmetric unit comprises one AB-dimer and one CC-dimer. To distinguish chains in the CC dimer, we designated the VP1 protomer proximal to the portal axis as chain D. Our model provides a detailed view of the virus-receptor interface (ED 4, SD 2, Supplemental Video 5). The footprint of each fJAM-A molecule is between 984 $Å^2$ (fJAM-A^D – the molecule bound primarily to chain D) and 1068 $Å^2$ (fJAM-A^A). Interactions at the interface between virus and receptor are largely electrostatic. Several hydrogen bonds are predicted to form between the capsid and receptor fragments, including between residues N444 and D445 in VP1 and Y51 and F54 in fJAM-A. These are of particular interest as a loop on the outer face of VP1 at residues 436-448 undergoes significant rearrangements upon fJAM-A binding, forming a cleft into which VP2 binds. It is also notable that K480 and K481 are identified as interacting with fJAM-A. These lysine residues lie within the putative metal binding site of VP1.

Aligning the P domains of the undecorated and fJAM-A-labelled models highlights the structural rearrangements within the P-domain following receptor engagement. The most striking structural changes take place in the P2 domains, in the above-mentioned 436-448 loops, which rise 3 Å towards the receptor (fig. 2a,b. Supplemental Video 6). In the S-domain following receptor engagement significant structural rearrangements at the icosahedral three-fold axis lead to the opening of a pore in the capsid shell (figure 2b-e). Consistent with the T=3 structure of the FCV capsid, the three-fold axes exhibit quasi-six-fold symmetry with six tyrosine residues (Y300) from chains B and C alternating about the axis. $Y300_B$ side-chains are tilted towards the capsid interior while those of $Y300_C$ are tilted towards the exterior. Upon receptor engagement the loops bearing these residues (293-307) fold outwards, resulting in the opening of a pore in the capsid shell that is ~1 nm in diameter (Supplemental Video 7). The presence of six tyrosine residues lining the three-fold axis is seen in all known vesivirus structures and appears to be conserved across the genus [21]. Structures of norovirus and rabbit haemorrhagic disease virus have phenylalanine residues at this site (ED6, SD3) [8,22]. A solvent-excluded surface representation of our atomic model shows that the counter-clockwise rotation of the capsomeres arranged about the portal vertex, following receptor binding, leads to a closing together of the P1 domains, forming a cup around the pore (figure 2d).

Twelve copies of the minor capsid protein VP2 are arranged about the unique three-fold axis to form a funnel shaped tube (fig. 3 and Supplemental Video 8). The asymmetric unit therefore includes four copies of VP2 (designated as chains I-L). The structure of VP2 includes three α-helices. The first and longest α-helix (*a*) makes up the body of the funnel

and extends from residue 18 to 62. The N-terminal 17 residues are not resolved and are distal to the capsid surface. Interestingly this region is characterised as being highly hydrophobic by Kyte-Doolittle analysis (ED6d). It has been shown previously that the N-terminal region of VP2 is critically important in FCV. Experiments to recover virus following mutagenesis of the viral genome identified two mutations, L7D and L7E, that gave rise to virus that was replication competent but non-infectious [3]. Likewise, transposon mediated insertional mutagenesis of murine norovirus revealed that the hydrophobic N-terminal region of VP2 in that virus is also intolerant of mutations (ED6e) [23]. These findings lead us to suggest that the distal tips of VP2 likely insert into the endosomal membrane.

VP2 is present in two distinct conformations that present different folds for residues 75-106. The two conformers alternate about the portal axis (six copies of each conformer). In conformer one (chains J and L), α-helices *b* (61-74) and *c* (91-106) bind to the capsid P domains via electrostatic interactions (ED7, SD4). In the second conformation of VP2 (designated as chains I and K) the C-terminal residues (75-106) do not bind VP1, rather they fold into the lumen of the portal, such that six symmetry-related C-terminal α-helices form an inner ring of fingers pointing away from the capsid surface. The C-terminal 6 residues of this conformer were not resolved. Conformer two barely contacts VP1 at all, the contact interface between this conformation and the capsid is ~150Å^2. VP2 is instead held within the portal-like complex primarily by hydrophobic interactions along the interface between the N-terminal α-helices (*a*). The C-terminal region of this conformer presents a largely negatively charged surface to the interior of the portal-like structure.

As FCV entry is dependent on acidification of the late endosome [13], we tested for release of viral genomes at low pH in the presence or absence of fJAM-A. Negative stain transmission electron microscopy and RNA release assays showed that in the presence of fJAM-A, virions disassemble at pH 4 and below (ED8, SD5). H+ concentration in the late endosome is thought to reach a pH of ~5 [24], thus virion disassembly under very low pH conditions is likely not physiologically relevant. These methods allowed us to establish the stoichiometry of receptor binding sufficient to induce structural changes in FCV. Measurements of RNA release from FCV virions in the presence of varying quantities of the fJAM-A ectodomain and at low pH showed that a 1:10 ratio of fJAM-A:VP1 is the minimum required to destabilise virions (ED9, SD6).

FCV engages fJAM-A such that a single receptor molecule binds to each VP1 monomer. We used small-angle X-ray scattering (SAXS) to calculate a low-resolution model of the protein solution structure. This showed that, like its human and murine orthologs, fJAM-A forms dimers in solution [9,10] (ED10, Supplemental Video 9). The FCV:fJAM-A interface is on the opposite side of the receptor to the D1:D1 dimerisation site. This site is however occluded by the D2 domain of symmetry-related fJAM-A molecules when bound to FCV [25]. Indeed, a significant contact interface arises between the D1 and D2 domains of the two receptor molecules when bound to the capsid (672 $Å^2$) (SD7). It is possible then that D1:D1 fJAM-A homodimers at the cell surface may be disrupted by binding of FCV. Interestingly, adenovirus fibre-knob protein has been shown to trigger endocytosis by disruption of homodimers of the immunoglobulin-like tight-junction protein CAR (coxsackie-adenovirus receptor) [26]. Thus, disruption of fJAM-A homodimers at the cell surface may be the mechanism by which FCV triggers endocytosis.

Taken together our data lead us to propose a mechanistic model of FCV entry and endosome escape: FCV binding to fJAM-A at the cell surface leads to internalisation by endocytosis, triggered by fJAM-A homodimer disruption. Enwrapping of the virion within the endosome leads to further binding of fJAM-A molecules, triggering conformational changes in the capsid that result in formation of the portal-like assembly at a unique vertex. The hydrophobic N-termini of VP2 insert into the endosomal membrane forming a channel through which the genome may be released. In our study viral genomic RNA remained associated with the capsid following receptor engagement, only being released at low pH as a consequence of virion disassembly. Further structural changes and possibly the action of an unknown cofactor may therefore be required to trigger release of the viral genome through the portal vertex *in vivo*.

It has long been known that large DNA-containing viruses, such as tailed bacteriophages and herpesviruses have unique portal-vertices that mediate genome release. Such features have not however been previously described in small RNA-containing viruses. Our discovery of a portal-like assembly at a unique vertex in caliciviruses therefore represents a paradigm shift in our understanding of the structure and biology of this class of viruses.

Supplementary information is linked to the online version of the paper at www.nature.com/nature.

Author contributions

MJC, IGG and DB conceived the study; MJC, MM and LA performed the experiments; MJC, OB and DB analysed the data; MG and DB performed validation; DB supervised the project; MJC and DB wrote the manuscript; all authors reviewed the manuscript.

Author information

Reprints and permissions information is available at www.nature.com/reprints. The authors declare no competing financial interests. Correspondence and requests for materials should be addressed to DB (David.bhella@glasgow.ac.uk).

Acknowledgments

CryoEM data in this study were collected at the University of Leeds, Astbury BioStructure Laboratory. The authors thank Sjors Scheres for advice on the application of focussed classification in Relion, Rebecca Thompson for microscopy support, Neil Ranson for microscope access and discussions, Joseph Hughes for advice on statistical analysis, Peter Stockley, Massimo Palmarini and John McLauchlan for discussions. We acknowledge Diamond Light Source for time on Beamline B21 under Proposal MX11651-24. IG is a Wellcome Senior Fellow (Ref: 207498/Z/17/Z). M.J.C. was supported by a PhD studentship from the UK Biotechnology and Biological Sciences Research Council (BBSRC WestBIO DTP: BB/J013854/1). D.B and M.M. are supported by the UK Medical Research Council (MC_UU_12014/7).

Figure Legends

Figure 1 Cryo-EM structures of FCV bound to fJAM-A reveal a portal-like assembly. An icosahedral three-dimensional reconstruction of the unlabelled virion structure was

calculated to an overall resolution of 3 Å. An isosurface thresholded view is shown coloured and filtered according to local resolution, showing that in the shell of the capsid the resolution approaches 2.8 Å, while on the outer faces of the protruding capsomeres the resolution is closer to 3.5 Å (a). Icosahedral reconstruction of receptor decorated FCV virions resulted in a lower overall resolution of 3.5 Å. The isosurface representation is similarly coloured and filtered according to local resolution, revealing that in this map the dimeric P-domain spikes and fJAM-A fragments are resolved at poorer than 4 Å resolution as a consequence of the receptor-induced conformational changes in this region (b). C3-symmetric 3D reconstruction of FCV decorated with fJAM-A following focussed classification analysis revealed the structure of a portal-like assembly at a unique three-fold symmetry axis. A wall-eyed stereo-pair view of the reconstruction along the icosahedral two-fold axis is shown coloured to highlight the portal vertex, (c). A close-up view of the portal assembly along the unique three-fold axis highlights the presence of a pore in the capsid shell at the centre of this symmetry axis (d). A cut-away view perpendicular to the portal axis (e). In panels c-e the map is coloured to highlight individual components: VP2 is coloured orange/red, VP1 dimers arranged about the portal vertex are coloured purple, associated fJAM-A molecules are coloured blue. The remaining density is radially coloured with a rainbow palette.

Figure 2 Conformational changes in VP1 following receptor engagement. Ribbon diagrams of the atomic models for FCV VP1 and fJAM-A following receptor engagement are shown for the AB-dimer (a) and CC-dimer (b). In panel (a), chain A is coloured pale pink, while chain B is coloured hot pink, fJAM-A^A is coloured blue, fJAM-A^B is coloured green. Overlaid on the structure are the aligned AB P-domains of the undecorated virus (purple), highlighting the

277 structural rearrangements that occur following fJAM-A binding. The most striking structural
278 change is the upwards movement of loop 436-448, indicated by black arrows. Panel (b)
279 shows the structure for the CC dimer, the portal proximal chain (now designated chain D) is
280 coloured dark purple, while the distal chain C is coloured pale purple, and fJAM-A molecules
281 are coloured blue. As in panel (a), the structure of VP1 in the absence of receptor is overlaid
282 (pink) to highlight the structural rearrangements that occur following receptor engagement.
283 This representation of the CC dimer also highlights the structural rearrangements that occur
284 in the S-domain leading to the opening of a pore in the capsid shell. Compare the
285 orientation of the 293-307 loop in chain D (red arrow) with the same loop in chain C.
286 Solvent-excluded surfaces are presented to show VP1 dimers arranged about the three-fold
287 symmetry axis in undecorated FCV (c), and fJAM-A labelled FCV at the portal axis (d) –
288 coloured by radius. A close-up view of the icosahedral three-fold axis in the undecorated
289 FCV reconstruction viewed from the capsid exterior (e) shows that this axis is surrounded by
290 six tyrosine (Y300) side chains that point to the centre of the symmetry axis. Three tyrosine
291 residues are each donated by chains B and C, that alternate about the symmetry axis
292 following the quasi-six-fold symmetry seen in a T=3 icosahedral structure. $Y300_B$ points
293 towards the capsid interior, while $Y300_C$ points outwards from the capsid surface. Following
294 receptor engagement, a portal complex assembles at a unique three-fold axis. At the centre
295 of this axis, a pore opens in the capsid surface by the folding outwards of loop 293-307 (f).
296 Panels (e) and (f) present both modelled coordinates (ribbon diagram in rainbow colour
297 scheme, atomic representation in pink) and the reconstructed density map (transparent
298 grey).
299

Figure 3 The structure of the VP2 portal-like assembly. A solvent-excluded surface representation of the portal vertex is presented viewed along the unique three-fold axis (a). Six dimers of VP1 are shown, AB (pink) and CD dimers (purple) alternate about the symmetry axis. On the outer surface of the P2 domain, fJAM-A molecules are bound (blue/green), with one receptor molecule binding to each VP1. The portal assembly, comprising twelve copies of the VP2 protein is shown as a ribbon diagram (orange/red). The portal-like assembly is viewed perpendicular to the portal axis and cutaway to show the interior features (b). The VP2 dodecameric portal structure is shown alone, viewed perpendicular to the portal axis (c). Two conformers of the molecule are seen in this assembly, conformer one (orange) and conformer two (red). The front-most VP2 chains K and L are shown in rainbow colouring, highlighting that the N-terminus of VP2 is distal to the capsid shell (c-d). VP2 has three α-helices designated *a*-*c* (e-f). The C-terminal residues (75-106) present different folds in the two conformers, with conformer one showing a well-ordered helix *c* that splays outwards, while the C-terminus of conformer two folds into the lumen of the portal.

Materials and Methods

Virus culture and purification

Feline calicivirus strain F9 was propagated in Crandell Reese Feline Kidney cells (CrFK) for 16 hours (all cell stocks were regular tested for Mycoplasma contamination). The cell debris was pelleted from the culture medium by centrifugation (1,500xg, 10 min at 4°C). The virus particles within the supernatant were pelleted by centrifugation at 20,000rpm for 2 hours at 4°C using a Surespin630 rotor. The pellets were resuspended in phosphate buffered saline (PBS) and the virus purified by centrifugation through a caesium chloride gradient (1.31-1.45g/ml) using a SW-41 Ti rotor at 28,000rpm for 8 hours and at 12°C. The purified virus particles were extracted from the gradient and pelleted by centrifugation at 20,000rpm for 2 hours at 4°C using an SW-41 Ti rotor. The resultant pellet was then resuspended in 100µl PBS and stored at 4°C until use.

Expression and purification of fJAM-A

The expression and purification of the soluble fJAM-A ectodomain was performed as previously described[11]. RNA was isolated from CrFK cells and the sequence encoding the signal peptide and ectodomains of fJAM-A was amplified by reverse transcription-PCR (RT-PCR). The PCR product was used to generate a eukaryotic expression plasmid termed pDEF:fJAM-A:Fc which contained the extracellular domains of fJAM-A with the Fc domain of human IgG1 fused at the C terminus. The fJAM-A and Fc domains were separated by a factor Xa cleavage site to allow downstream removal of the Fc tag. Chinese hamster ovary cells stably expressing the soluble fJAM-A:Fc fusion protein were generated and soluble fJAM-A:Fc protein purified from tissue culture supernatant using protein A Sepharose. Monomeric

fJAM-A was generated by factor Xa cleavage of fJAM-A:Fc, removal of factor Xa by using Xarrest agarose (Novagen), and removal of the released Fc domain by protein A dynabeads.

Sequencing of FCV VP1 and VP2 ORFs

The sequences for the FCV capsid protein ORFs were determined to facilitate atomic model building. RT-PCR was used to isolate the relevant DNA for sequencing using the Sanger method, performed at the MRC Protein Phosphorylation Unit, University of Dundee.

Primers were designed based on published FCV Strain LLK VP1 and VP2 sequence data (Genbank U07131[27]) as follows:

VP RT primer : 5'-ttaggcgcaggtgcggcagc-3'

VP1 PCR1 5'-atgtgctcaacctgcgctaacgtgct-3

VP1 PCR2 5'-tcataacttagtcatgggactcctaa-3'

VP2 PCR1 5'-atgaattcaatattaggcctgatt-3'

VP2 PCR2 5'-aattttaaacaaatttttatatga-3'

RNA was extracted from 140 µl of FCV strain F9 infected cell culture medium using a Qiagen QiaAMP Viral RNA mini kit according to the manufacturers protocol. The purified RNA was reverse transcribed using a Superscript IV RT kit (Thermo Fisher) and VP RT primer in a 20 µl reaction volume according to the manufacturer's protocol. PCR was carried out on 6 µl of the RT reaction using the Q5 High Fidelity PCR kit (NEB). VP1 was amplified using primers VP1 PCR1 and VP1 PCR2, and VP2 was amplified using primers VP2 PCR1 and VP2 PCR2. PCR products were purified using agarose gel electrophoresis and the Geneclean Turbo kit (MPBio).

Negative stain electron microscopy

Purified FCV particles were incubated with the soluble ectodomain of fJAM-A at pH7 or pH3 for 1 h at 4°C. FCV particles, both undecorated and labelled with fJAM-A, were imaged by negative stain transmission electron microscopy. 5 µl of virus preparation was loaded onto a freshly glow-discharged continuous carbon TEM grid. The grid was washed in two 20µl droplets of 2% uranyl acetate, drained and dried at room temperature. The grids were then imaged in a JEOL 1200 EX II transmission electron microscope equipped with a GATAN Orius camera.

Cryo-electron microscopy

Purified FCV particles were incubated with the soluble ectodomain of fJAM-A for 1 h at 4°C. The undecorated and decorated virions were then prepared for cryo-electron microscopy by loading 5µl onto freshly glow-discharged, carbon coated c-flat holey carbon grids (CF-22-4C, Protochips Inc.) in a Vitrobot vitrification robot (FEI) held at 4°C and 100% humidity. Grids were blotted for 4 seconds prior to being frozen by plunging into a bath of liquid nitrogen-cooled liquid ethane.

Vitrified specimens were imaged at low temperature in a Thermo-Fisher Titan Krios equipped with a Falcon III detector. The column was operated at 300 keV accelerating voltage and a nominal magnification of 75,000x resulting in a pixel size of 1.065 Å/pixel. Each micrograph was recorded as a movie of 50 individual fractions with a total dose of 63 e/Å^2. Automated data collection was performed using EPU software. 5,198 micrographs of

FCV and 13,865 micrographs of FCV-fJAM-A were recorded. Data collection was performed at the Astbury BioStructure Laboratory, University of Leeds.

Three-dimensional image reconstruction

Micrograph stack files were corrected for drift using MotionCor2[28] and defocus estimation performed by Gctf[29] as implemented in Relion 2.1[30]. 59,531 undecorated particles were automatically picked from 5198 micrographs and 129,884 fJAM-A decorated particles from 13,865 micrographs. Particle images were subjected to both 2D and 3D classification to exclude false-positives and damaged particles. Final datasets of 41,436 undecorated and 71,671 fJAM-A decorated virions were subjected to 3D refinement to calculate final icosahedrally averaged three-dimensional reconstructions. These were then subjected to post-processing and local resolution analysis in Relion 2.1 to determine both final resolution and optimal sharpening parameters. Maps were visualised using UCSF Chimera [31] and ChimeraX and coloured according to local resolution, unless otherwise specified.

Model based classification

To attempt to separate fJAM-A decorated FCV virions into separate classes based on the extent of conformational change they had undergone, 3D classification was performed in Relion 2.1 using our previously published structures as starting models[12].

Focussed classification

To resolve the structures of individual asymmetric features we employed a focussed classification approach in Relion 2.1 [14-16]. Briefly, following 3D refinement with imposition of icosahedral symmetry, the symmetry of the data set was expanded such that each particle

was assigned 60 orientations corresponding to its icosahedrally redundant views. A cylindrical mask was prepared to exclude all of the capsid structure except the area of interest, using SPIDER [32]. 3D classification was then performed without orientation refinement. Thus, a single capsomere or symmetry axis was reconstructed, and classification was performed to resolve structural differences.

Atomic model building

Atomic models were built using Coot [33], the CCP-EM [34] suite and Phenix [35]. The structure for VP1 of FCV in the undecorated virus was built starting from our previously calculated homology model [11]. The structure was manually edited in Coot to correct the sequence and improve the correspondence to our EM density map. This was followed by rounds of iterative real-space refinement in Phenix. To build an atomic model of VP1 in our receptor-bound models, the P-domains and S-domains were docked independently as rigid bodies using UCSF Chimera [31]. The models were then manually edited and iteratively refined as above. Likewise, the structure for fJAM-A was built starting from our previously calculated homology model and refined using Coot and Phenix. The structure of VP2 was manually built *ab initio* in Coot and refined using Phenix. Model validation was performed using MolProbity [36], as implemented in Phenix. Modelling of metal ions was validated using the checkmymetal server (https://csgid.org/csgid/metal_sites) [19]. Interactions between fJAM-A and VP1 were characterised for each of the four VP1 chains in the asymmetric unit using tools in UCSF Chimera[31] and the 'Protein interfaces, surfaces and assemblies' (PISA) service at the European Bioinformatics Institute (http://www.ebi.ac.uk/pdbe/prot_int/pistart.html) [37]. Protein sequence alignments were calculated using Clustal Omega (https://www.ebi.ac.uk/Tools/msa/clustalo/) [38].

RNA release assay

Equal concentrations of FCV and fJAM-A ectodomain were combined in Tris buffer of the appropriate pH. 10µl Syto9 nucleic acid binding dye (ThermoFisher Scientific) was added to a final volume of 100µl in a black 96-well plate. For positive controls, 550 ng FCV RNA was added in place of the FCV and fJAM-A samples. Fluorescence readings were collected every 5 minutes over a period of 4 hours using a PHERAstar *FS* (BMG labtech) plate reader equipped with a 485/520 filter cube. Data were normalised to the corresponding samples containing only FCV and Syto9. Plots of normalised fluorescence against time were evaluated by linear regression to determine whether the slope in each plot was significantly different from zero, using GraphPad Prism.

Small Angle X-ray Scattering (SAXS)

The fJAM-A ectodomain was dialysed into PBS containing 0.01% sodium azide, 1% sucrose and 10 mM potassium nitrate and samples taken to the Diamond Light Source (Oxfordshire, UK) where high-pressure liquid chromatography (HPLC) small angle X-ray scattering (SAXS) data were acquired. The HPLC column (Superdex 200 (GE Healthcare)) was equilibrated with buffer for 1 hour, the sample loaded onto the column from a 96-well plate and the diffraction data collected. Eight 60-second frames of data, for which the radius of gyration (Rg) was observed to be constant, were selected for further processing with PRIMUS [39], part of the ATSAS program suite for small-angle scattering data analysis from biological macromolecules [40]. A Guinier region was observed between $0.26 \leq qRg \leq 1.29$ Å^2 (where q is the momentum transfer ($4\pi\sin(\Theta)/\lambda$)) giving Rg = 30.7 Å. The particle distance distribution function (p(r) *versus* r, where r is the real-space distance) was evaluated using GNOM [41] with

a maximum dimension of 102.8 Å. An *ab initio* envelope was computed from p(r) *vs* r using DAMMIF [42]. The dimeric model of human fJAM-A ectodomain (PDB-1NBQ [10]) was fitted into the SAXS envelope using UCSF Chimera [31].

Data availability statement

The icosahedral reconstruction of undecorated FCV and the C3-symmetrised reconstruction of FCV-fJAM-A are deposited in the EM databank with accession numbers EMD-0054 and EMD-0056 respectively. The atomic coordinates for the FCV capsid asymmetric unit (VP1) are deposited in the protein data bank with accession number PDB-6GSH. The atomic coordinates for the FCV-fJAM-A portal vertex (VP1, VP2 and fJAM-A) are deposited in the protein data bank with accession number PDB-6GSI. Motion corrected micrographs of undecorated and fJAM-A labelled FCV (the raw data) are deposited in the EMPIAR data bank with accession numbers EMPIAR-10192 and EMPIAR-10193 respectively.

Extra Data Legends

ED 1

CryoEM of FCV decorated with soluble f-JAM-A. Cryogenic electron microscopy of feline calicivirus (FCV) strain F9 virions both unlabelled (a) and decorated with soluble ectodomain fragments of feline-junctional adhesion molecule A (fJAM-A) (d), scale bar is 100 nm. Icosahedral three-dimensional reconstructions were calculated. A central section through the reconstructed density map for the unlabelled virion shows that both the shell (S) and protruding spike (P) domains were sharply resolved (b). A central slice through the reconstruction of receptor decorated FCV virions shows that while the capsid shell is sharply resolved, the P-domains and fJAM-A components are blurred as a consequence of the receptor-induced conformational changes in this region (e). Gold-standard Fourier shell correlation plots for the icosahedral reconstructions show a nominal resolution of 3 Å for unlabelled FCV (c) and 3.5 Å for the receptor decorated structure (f).

ED 2

Conformational changes in FCV following receptor engagement, revealed by focussed classification. 3D reconstruction of FCV decorated with soluble fJAM-A ectodomain, in the pre-conformational change state. Model based classification was used to identify a small subset of particles (493/71,671) that were found not to have undergone the rotation of capsomeres usually induced by receptor engagement. These data gave a reconstruction with a nominal resolution of 6 Å. The surface-rendered representation is coloured and filtered according to local resolution (a). A central section through the map revealed density that was less blurred than in particles showing capsomere rotation (compare figure ED2b with figure ED1e). To resolve the range and extent of capsomere movement following receptor engagement, focussed classification was applied to reconstruct individual capsomeres at the AB- and CC-dimer positions. Montages of images showing individual capsomeres reveal the range of conformations present at the AB-dimer (c) and CC-dimer (d) positions. The first panel of each montage (top-left) shows the unlabelled dimer, the second panel (top, second from left) shows the class presenting a pre-conformational change state, remaining panels show the extent of conformational changes at each capsomere. Surface representations are filtered and coloured according to local resolution (Å – see colour keys). Red arrows highlight the position of a novel feature that we have shown to be VP2.

ED 3

A portal-like assembly located at a unique three-fold axis. Sections through the reconstructed portal-like assembly and virion viewed along the three-fold symmetry axis of the portal assembly. Viewed through the distal tips of the structure (a), viewed through the middle of the structure, also showing fJAM-A density (b) and viewed through the base of the assembly, also showing VP1 P-domain density (c). A transverse section through the virion along the portal axis shows the extent of the assembly and the presence of blurred density extending from the distal tip (d). We can also see the clear opening of a pore in the capsid shell at the portal-vertex (red arrow), which is not present at the opposite non-portal vertex (white arrow). Histogram to show the number of views contributed to the portal reconstruction by each particle (e). Focussed classification was used to identify and reconstruct the unique portal axis. Each of the twenty, three-fold symmetry axes present in every particle image was, in-turn, sampled such that it was oriented to lie within a 3D

cylindrical mask that covered a single three-fold axis of the icosahedral reference structure. Furthermore, each of the particle's three-fold axes were tested in three possible orientations, owing to the C3 symmetry of that axis. Thus, 60 views were evaluated for each particle, corresponding to the redundancy of an icosahedral symmetric object. Our data set of 71,671 particle images therefore gave rise to 4,300,260 views that were tested. 234,076 particle views were assigned to the class in which the portal assembly was present, corresponding to 5.44% of the dataset. This is consistent with each particle having a single portal at a unique three-fold axis, as there are 20 three-fold symmetry axes per virion. The median number of views for each particle is indeed 3, consistent with the C3 symmetry of the assembly. Only 58,510 particles contributed to the reconstruction however, suggesting that ~20% of particles had either not assembled their portals, or the particle orientations were such that the portal was not discernible. In total 35,714 particles (61%) were found to contribute three views (i.e. contain a single portal) while 12,974 particles (22%) were found to contribute six views (two portals). 1,706 particles (2%) contributed nine views (three portals). We should assume a degree of error in the assignment of particles to each class however. Those particles that were found to contribute numbers of views that are not multiples of three are likely not entirely correctly classified. Moreover, particles presenting six or nine views might also be misclassified. The focussed classification analysis sorts data according to the presence of small/weak differences that are superimposed onto the projected density of the entire icosahedral object. Nonetheless, overall these data indicate that the most populous class of particles present a single portal at a unique three-fold axis.

ED 4

The structure of FCV VP1 showing sites of metal binding and receptor engagement. Ribbon diagram to show the atomic model of the FCV strain F9 major capsid protein VP1, calculated by modelling the protein sequence (SD 1) into the icosahedral reconstruction of the undecorated virion (a). The AB-dimer is shown. Chain A is coloured pale pink, chain B is presented in rainbow representation (N-terminus blue, C-terminus red). A side-view of the dimeric capsomere is labelled to identify the shell (S) and protruding (P1 and P2) domains. The S domain shows the characteristic 'β-jellyroll' motif seen in all calicivirus structures solved to date. A top-view of the VP1 dimer is shown with a box to highlight the location of a putative metal ion (b). A close-up view of this region is presented identifying the

coordinating interactions within the metal binding site. Based on the distances measured for these interactions we suggest that this metal ion may be potassium (c). A recent mutational analysis of FCV VP1 fJAM-A binding identified several amino-acid residues within or close to the coordinating sphere of this metal-ion, that were critical to virus infectivity. Viruses in which these sites were mutated (I482, K480 and H516) were able to both assemble capsids and bind to fJAM-A but were not infectious. Sequence analysis also highlighted differences between VS-FCV and non-VS strains within this region, including residue D479, which in VS-FCV strain 5 is an asparagine residue and is oriented away from the site of metal binding we see in strain F9 (d - PDB 3M8L). Furthermore, Q474 and K481 are oriented in a manner that is not compatible with metal-binding. The deposited structure factors for PDB 3M8L were downloaded for VS-FCV strain 5. Close inspection of the density revealed no evidence of metal binding. The atomic model for VP1 chains A (pale pink) and B (hot pink) of FCV decorated with fJAM-A^{A} (the molecule bound primarily to chain A - blue) and fJAM-A^{B} (the molecule bound primarily to chain B - green) is shown as a solvent excluded surface (e). The interface is exposed by opening the fJAM-A/VP1 surfaces like a book. Contact atoms are highlighted in the colour of the molecule they are interacting with (f). Coulombic surface colouring highlights the charge distribution (g), the contact interface is indicated by a black outline.

ED5

CryoEM form (no legend).

ED 6

Structures of the icosahedral three-fold axes in related caliciviruses and hydrophobicity analysis of VP2. Ribbon diagrams to show the icosahedral three-fold symmetry axes of other known calicivirus structures. Similar to FCV, the vesivirus San Miguel Sealion virus (PDB 2GHT) has six tyrosine residues (a). Rabbit haemorrhagic disease virus (b – PDB 2J1P) and norovirus (c – PDB 1IHM) both have phenylalanines.

The N-terminal region of VP2 is highly hydrophobic, leading us to suggest it may insert into the endosomal membrane. Kyte-Doolittle plots showing the hydrophobicity profile of VP2 for FCV (d) and MNV (e). A positive number indicates a predominantly hydrophobic region (Figure generated using Expasy Protscale - https://web.expasy.org/protscale/). Mutational

582 studies of VP2 in FCV and MNV have both shown that the hydrophobic N-terminal region is
583 intolerant of mutagenesis. Analyses of the VP2 sequences for human norovirus (strain
584 GI/Human/United States/Norwalk/1968) and rabbit haemorrhagic disease virus also show
585 the presence of a hydrophobic N-terminus indicating that this feature is conserved across
586 the *Caliciviridae* (data not shown).
587
588 **ED 7**
589 *The structure of FCV VP2 and interactions with the capsid surface.* Wall-eyed stereo pair
590 images of VP2 to show the folds of the two conformers that are seen to alternate about the
591 three-fold portal axis and highlight the interactions between conformer one (orange) and
592 the major capsid protein VP1. A dimer of VP2 showing the two conformations is presented
593 viewed from the portal interior, α-helices are labelled. The poorly-ordered C-terminal helix *c*
594 of conformer two can be seen leaning towards the viewer (a). A solvent-excluded surface
595 representation of this view, coloured to show surface potential (negative = red, positive =
596 blue), shows that the C-terminal region of conformer two presents a negatively charged
597 surface to the portal interior (black arrow – (b)). Panels (c) and (d) show the same VP2 dimer
598 rotated 180^{o} about the vertical axis, the outward facing C-terminal helix of conformer one is
599 now leaning towards the viewer. Interestingly, both helix *b* and helix *c* in this conformer
600 present positively charged surfaces (black and red arrows respectively), which bind to
601 negatively charged clefts on the capsid surface (e). Two binding sites are present on the
602 capsid surface, helix *c* binds to the P1 domains of both VP1 molecules in each dimeric
603 capsomere arranged about the portal axis (AB or CD) (f). The *bc* loops (residues 75-90) wrap
604 across the surface of the adjacent VP1 molecule laying closest to the portal axis (chains D or
605 B respectively) and helix *b* binds to a cleft on the adjacent portal proximal VP1 molecule in
606 the P2 domain (g). This binding site is opened up by the upwards movement of loop 436-448
607 following fJAM-A binding. Ribbon diagrams of the portal proximal VP1 molecule (in this case
608 chain D) are shown for both fJAM-A decorated (purple) and unlabelled (blue) VP1, showing
609 that without the structural rearrangements of loop 436-448 brought about by receptor
610 binding, the helix and loop (450-460) laying immediately below clashes with helix *b* of VP2
611 (yellow arrow) (h). Thus, each of the VP2 molecules in the first conformation binds to three
612 VP1 molecules: $VP2_J$ is anchored to $VP1_{AB}$ in the P1 binding site. The *bc* loop then wraps
613 across the surface of $VP1_D$ and helix *b* inserts into the second binding site, in the P2 domain

614 of $VP1_D$. Likewise, helix *c* of $VP2_L$ binds to $VP1_{CD}$ in the P1 cleft. It then folds across the face
615 of $VP1_B$ binding into the second interaction site on that protomer.
616
617 **ED 8**
618 *FCV disassembles at low pH in the presence of fJAM-A.* RNA release assay plots showing
619 fluorescence induced by release of RNA from FCV virions in the presence of fJAM-A and
620 under varying pH conditions (a). These data show that at pH4 or below, FCV particles
621 labelled with fJAM-A release their RNA. Measurements were taken from distinct samples
622 (n=3) and normalised data is shown with error bars representing the standard deviation
623 (*** p=0.0002, **** p=<0.0001 – supplemental data 5). Negative-stain transmission
624 electron microscopy of purified FCV virions showed that fJAM-A decorated FCV virions
625 release their RNA at low pH as a consequence of capsid disassembly. Micrographs are
626 shown for FCV alone at pH3 (b) and pH7 (d) and FCV decorated with soluble fJAM-A at pH3
627 (c) or pH 7 (e). Virions can be clearly seen in both experiments performed at neutral pH,
628 however at pH3 and in the presence of fJAM-A, no virions were seen. FCV was incubated for
629 1h in the presence or absence of fJAM-A and at neutral or low pH.
630
631 **ED 9**
632 *Stoichiometry analysis of fJAM-A binding to VP1 leading to capsid destabilisation.* RNA
633 release assay plots showing the RNA released by virions at low pH and in the presence of
634 varying ratios of fJAM-A to VP1 (a). Clear evidence of RNA release is seen at ratios down to
635 1:9, while between 1:11 and 1:14 the assay is equivocal. Below 1:16 there is no evidence of
636 RNA release. Measurements were taken from distinct samples (n=3) and normalised data is
637 shown with error bars representing the standard deviation (*** p=0.0002, **** p=<0.0001
638 – supplemental data 6). Negative stain TEM imaging of FCV virions in the presence of
639 differing ratios of fJAM-A:VP1 and at pH 7 and pH3 (b-i). At a ratio of fJAM-A:FCV-VP1 of 1:9,
640 intact virions are seen at pH7 (b), while at pH3 no virions were seen (c). Likewise, at a ratio
641 of 1:10 virions were seen to disassemble at pH3 (pH7 - d, pH3 - e). At a ratio of 1:11 (pH7 - f,
642 pH3 – g), disrupted or partially disassembled particles were visible at pH3 while at a ratio of
643 1:12 particles were intact at both neutral and low pH (pH7 - h, pH3 – i). In each case FCV
644 was incubated for 1h under the relevant experimental conditions. These images show that a
645 ratio of 1 fJAM-A molecule to 10 capsid proteins is sufficient to destabilise capsids, causing

646 them to completely disassemble at low pH. Imaging disassembled virions revealed the
647 presence of small dense balls of density, that we interpret as being condensed viral RNA
648 (white arrows - c, e, g, i). These were sometimes also seen in intact preparations of FCV at
649 neutral pH (red arrow - h).
650

ED Fig 10

fJAM-A is a dimer in solution. Small angle X-ray scattering was used to calculate a low-resolution envelope for fJAM-A ectodomain fragments in solution (a), this closely matched the structure of the human JAM-A homodimer (PDB 1NBQ). The atomic model of hJAM-A is docked and shown as a ribbon diagram (b,c) and solvent-excluding surface (c). The homodimerisation interface (red, d) is on the opposite face of D1 to the FCV binding site (pink, e). In fJAM-A molecules bound to the P2 domains of FCV VP1 dimers, the homodimerisation sites at D1 are occluded by the D2 domains of the symmetry related bound receptor molecules (f,g). Indeed, an alternate dimerisation interface arises between D1 and D2 domains of bound molecules.

References

Main Text

1 Glass, P. J. *et al.* Norwalk virus open reading frame 3 encodes a minor structural protein. *J Virol* **74**, 6581-6591 (2000).

2 Wirblich, C., Thiel, H. J. & Meyers, G. Genetic map of the calicivirus rabbit hemorrhagic disease virus as deduced from in vitro translation studies. *J Virol* **70**, 7974-7983 (1996).

3 Sosnovtsev, S. V., Belliot, G., Chang, K. O., Onwudiwe, O. & Green, K. Y. Feline calicivirus VP2 is essential for the production of infectious virions. *J Virol* **79**, 4012-4024, doi:10.1128/JVI.79.7.4012-4024.2005 (2005).

4 Carstens, E. B. Ratification vote on taxonomic proposals to the International Committee on Taxonomy of Viruses (2009). *Arch Virol* **155**, 133-146, doi:10.1007/s00705-009-0547-x (2010).

5 Kapikian, A. Z. *et al.* Visualization by immune electron microscopy of a 27-nm particle associated with acute infectious nonbacterial gastroenteritis. *J Virol* **10**, 1075-1081 (1972).

6 Pesavento, P. A., Chang, K. O. & Parker, J. S. Molecular virology of feline calicivirus. *Vet Clin North Am Small Anim Pract* **38**, 775-786, vii, doi:10.1016/j.cvsm.2008.03.002 (2008).

7 Makino, A. *et al.* Junctional adhesion molecule 1 is a functional receptor for feline calicivirus. *J Virol* **80**, 4482-4490, doi:10.1128/JVI.80.9.4482-4490.2006 (2006).

8 Prasad, B. V. *et al.* X-ray crystallographic structure of the Norwalk virus capsid. *Science* **286**, 287-290 (1999).

9 Kostrewa, D. *et al.* X-ray structure of junctional adhesion molecule: structural basis for homophilic adhesion via a novel dimerization motif. *EMBO J* **20**, 4391-4398, doi:10.1093/emboj/20.16.4391 (2001).

10 Prota, A. E. *et al.* Crystal structure of human junctional adhesion molecule 1: implications for reovirus binding. *Proc Natl Acad Sci U S A* **100**, 5366-5371, doi:10.1073/pnas.0937718100 (2003).

11 Bhella, D., Gatherer, D., Chaudhry, Y., Pink, R. & Goodfellow, I. G. Structural insights into calicivirus attachment and uncoating. *J Virol* **82**, 8051-8058, doi:10.1128/JVI.00550-08 (2008).

12 Bhella, D. & Goodfellow, I. G. The cryo-electron microscopy structure of feline calicivirus bound to junctional adhesion molecule A at 9-angstrom resolution reveals receptor-induced flexibility and two distinct conformational changes in the capsid protein VP1. *J Virol* **85**, 11381-11390, doi:10.1128/JVI.05621-11 (2011).

13 Stuart, A. D. & Brown, T. D. Entry of feline calicivirus is dependent on clathrin-mediated endocytosis and acidification in endosomes. *J Virol* **80**, 7500-7509, doi:10.1128/JVI.02452-05 (2006).

14 McElwee, M., Vijayakrishnan, S., Rixon, F. & Bhella, D. Structure of the herpes simplex virus portal-vertex. *PLoS Biol* **16**, e2006191, doi:10.1371/journal.pbio.2006191 (2018).

15 Scheres, S. H. Processing of Structurally Heterogeneous Cryo-EM Data in RELION. *Methods Enzymol* **579**, 125-157, doi:10.1016/bs.mie.2016.04.012 (2016).

16 Zhou, M. *et al.* Atomic structure of the apoptosome: mechanism of cytochrome c- and dATP-mediated activation of Apaf-1. *Genes Dev* **29**, 2349-2361, doi:10.1101/gad.272278.115 (2015).

17 Sun, L. *et al.* Icosahedral bacteriophage PhiX174 forms a tail for DNA transport during infection. *Nature* **505**, 432-435, doi:10.1038/nature12816 (2014).

18 Ossiboff, R. J., Zhou, Y., Lightfoot, P. J., Prasad, B. V. & Parker, J. S. Conformational changes in the capsid of a calicivirus upon interaction with its functional receptor. *J Virol* **84**, 5550-5564, doi:10.1128/JVI.02371-09 (2010).

19 Zheng, H. *et al.* CheckMyMetal: a macromolecular metal-binding validation tool. *Acta Crystallogr D Struct Biol* **73**, 223-233, doi:10.1107/S2059798317001061 (2017).

20 Lu, Z., Ledgerwood, E. D., Hinchman, M. M., Dick, R. & Parker, J. S. L. Conserved Surface Residues on the Feline Calicivirus Capsid Are Essential for Interaction with Its Receptor Feline Junctional Adhesion Molecule A (fJAM-A). *J Virol* **92**, doi:10.1128/JVI.00035-18 (2018).

21 Chen, R., Neill, J. D., Estes, M. K. & Prasad, B. V. X-ray structure of a native calicivirus: structural insights into antigenic diversity and host specificity. *Proc Natl Acad Sci U S A* **103**, 8048-8053, doi:10.1073/pnas.0600421103 (2006).

22 Wang, X. *et al.* Atomic model of rabbit hemorrhagic disease virus by cryo-electron microscopy and crystallography. *PLoS Pathog* **9**, e1003132, doi:10.1371/journal.ppat.1003132 (2013).

23 Thorne, L., Bailey, D. & Goodfellow, I. High-resolution functional profiling of the norovirus genome. *J Virol* **86**, 11441-11456, doi:10.1128/JVI.00439-12 (2012).

24 Scott, C. C. & Gruenberg, J. Ion flux and the function of endosomes and lysosomes: pH is just the start: the flux of ions across endosomal membranes influences endosome function not only through regulation of the luminal pH. *Bioessays* **33**, 103-110, doi:10.1002/bies.201000108 (2011).

25 Bhella, D. The role of cellular adhesion molecules in virus attachment and entry. *Philos Trans R Soc Lond B Biol Sci* **370**, 20140035, doi:10.1098/rstb.2014.0035 (2015).

26 Salinas, S. *et al.* Disruption of the coxsackievirus and adenovirus receptor-homodimeric interaction triggers lipid microdomain- and dynamin-dependent endocytosis and lysosomal targeting. *J Biol Chem* **289**, 680-695, doi:10.1074/jbc.M113.518365 (2014).

Methods

27 Seal, B. S. & Neill, J. D. Capsid protein gene sequence of feline calicivirus isolates 255 and LLK: further evidence for capsid protein configuration among feline caliciviruses. *Virus Genes* **9**, 183-187 (1995).

28 Zheng, S. Q. *et al.* MotionCor2: anisotropic correction of beam-induced motion for improved cryo-electron microscopy. *Nat Methods* **14**, 331-332 (2017).

29 Zhang, K. Gctf: Real-time CTF determination and correction. *J Struct Biol* **193**, 1-12, doi:10.1016/j.jsb.2015.11.003 (2016).

30 Scheres, S. H. RELION: implementation of a Bayesian approach to cryo-EM structure determination. *J Struct Biol* **180**, 519-530, doi:10.1016/j.jsb.2012.09.006 (2012).

31 Pettersen, E. F. *et al.* UCSF Chimera--a visualization system for exploratory research and analysis. *J Comput Chem* **25**, 1605-1612, doi:10.1002/jcc.20084 (2004).

32 Frank, J. *et al.* SPIDER and WEB: processing and visualization of images in 3D electron microscopy and related fields. *J Struct Biol* **116**, 190-199, doi:10.1006/jsbi.1996.0030 (1996).

33 Emsley, P. & Cowtan, K. Coot: model-building tools for molecular graphics. *Acta Crystallogr D Biol Crystallogr* **60**, 2126-2132, doi:10.1107/S0907444904019158 (2004).

34 Burnley, T., Palmer, C. M. & Winn, M. Recent developments in the CCP-EM software suite. *Acta Crystallogr D Struct Biol* **73**, 469-477, doi:10.1107/S2059798317007859 (2017).

35 Adams, P. D. *et al.* PHENIX: a comprehensive Python-based system for macromolecular structure solution. *Acta Crystallogr D Biol Crystallogr* **66**, 213-221, doi:10.1107/S0907444909052925 (2010).

36 Chen, V. B. *et al.* MolProbity: all-atom structure validation for macromolecular crystallography. *Acta Crystallogr D Biol Crystallogr* **66**, 12-21, doi:10.1107/S0907444909042073 (2010).

37 Krissinel, E. & Henrick, K. Inference of macromolecular assemblies from crystalline state. *J Mol Biol* **372**, 774-797, doi:10.1016/j.jmb.2007.05.022 (2007).

38 Sievers, F. *et al.* Fast, scalable generation of high-quality protein multiple sequence alignments using Clustal Omega. *Mol Syst Biol* **7**, 539, doi:10.1038/msb.2011.75 (2011).

39 Konarev, P. V., Volkov, V. V., Sokolova, A. V., Koch, M. H. J. & Svergun, D. I. PRIMUS: a Windows PC-based system for small-angle scattering data analysis. *Journal of Applied Crystallography* **36**, 1277-1282 (2003).

40 Franke, D. *et al.* ATSAS 2.8: a comprehensive data analysis suite for small-angle scattering from macromolecular solutions. *J Appl Crystallogr* **50**, 1212-1225, doi:10.1107/S1600576717007786 (2017).

41 Svergun, D. I. Determination of the Regularization Parameter in Indirect-Transform Methods Using Perceptual Criteria. *Journal of Applied Crystallography* **25**, 495-503 (1992).

42 Franke, D. & Svergun, D. I. DAMMIF, a program for rapid ab-initio shape determination in small-angle scattering. *J Appl Crystallogr* **42**, 342-346, doi:10.1107/S0021889809000338 (2009).

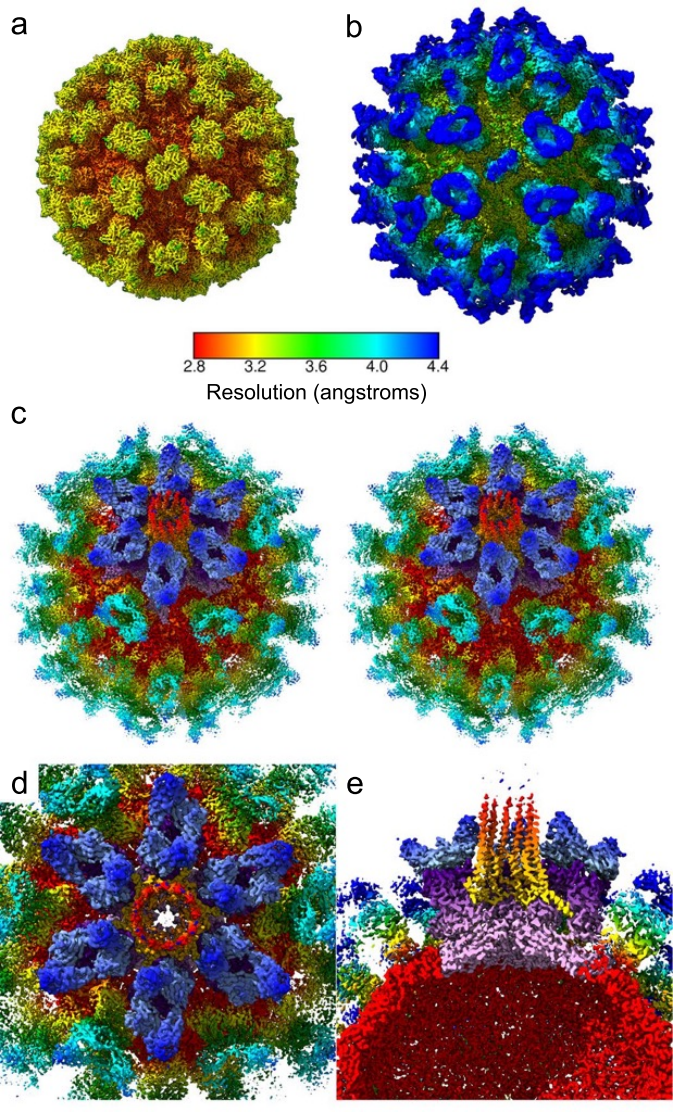
a
b
2.8
3.2
3.6
4.0
4.4
Resolution (angstroms)
c
d
e

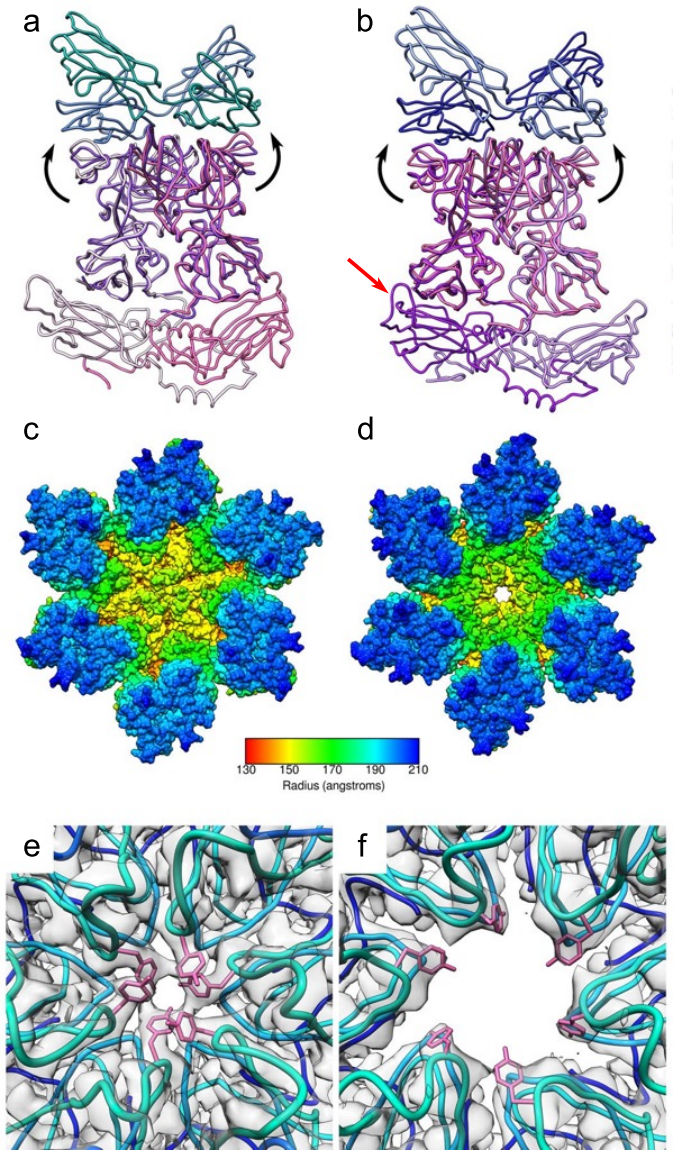
a
b
c
d
130
150
170
190
210
Radius (angstroms)
e
f

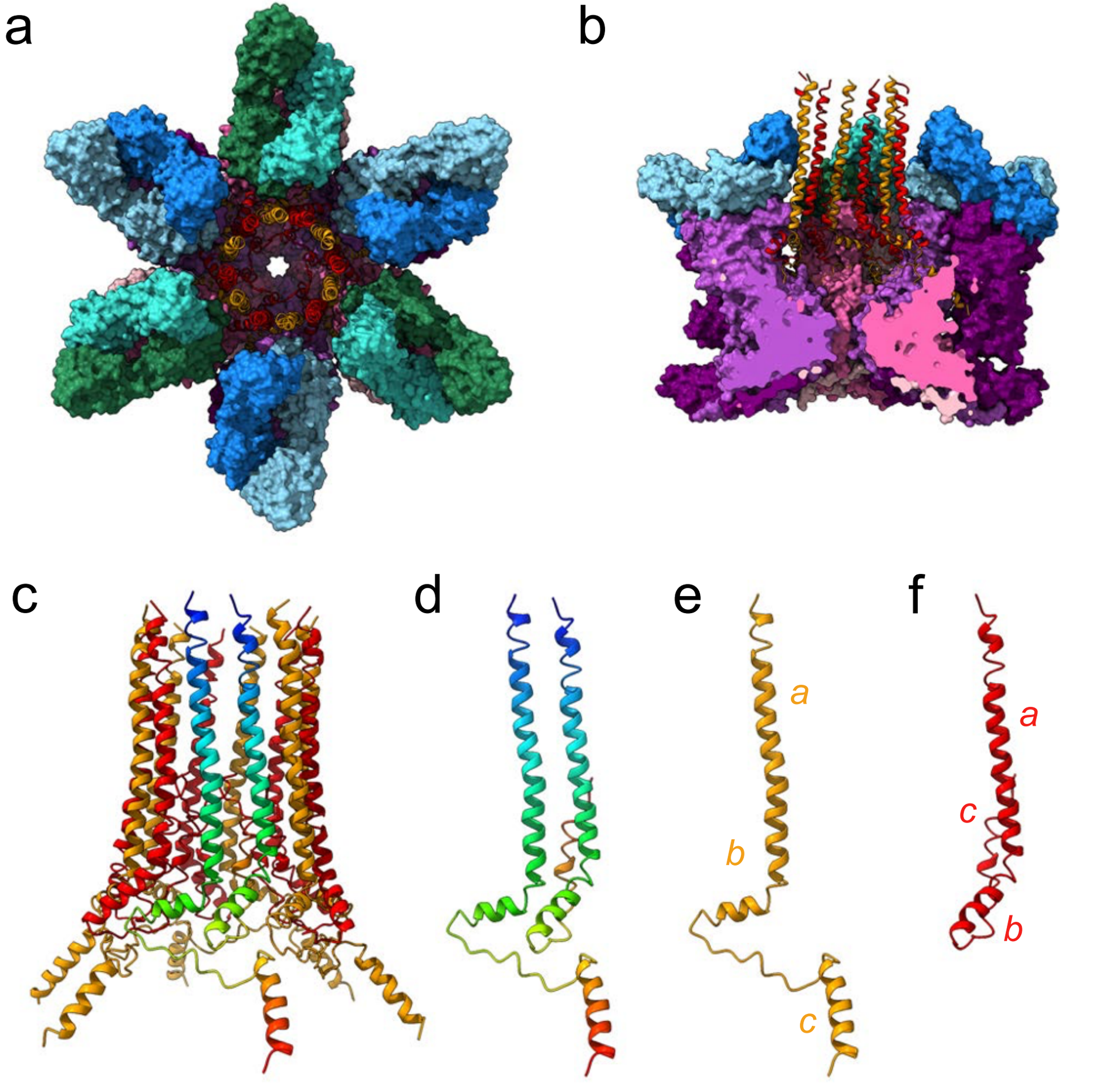
a
b
c
d
e
f
a
b
c
a
c
b

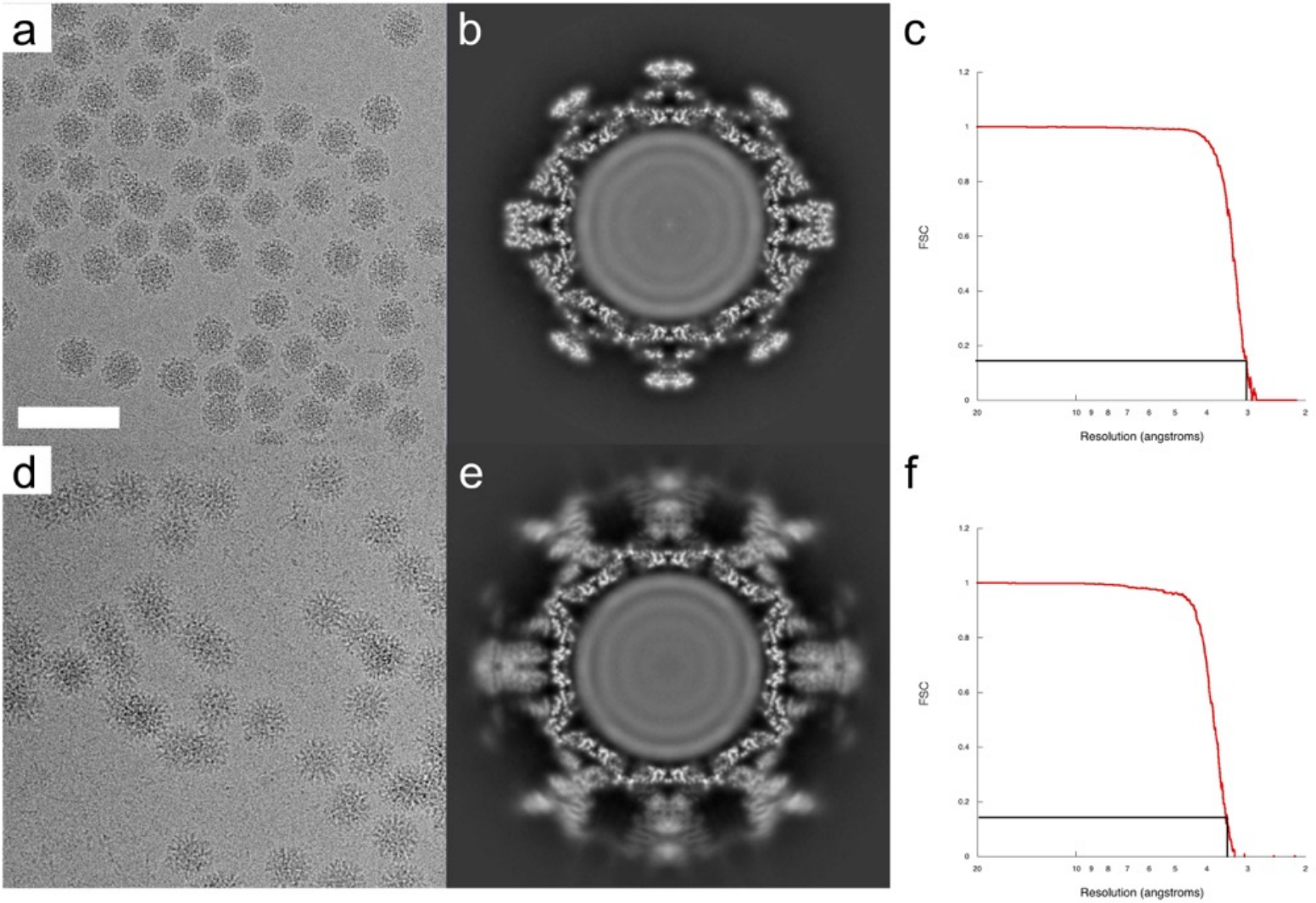
a
b
c
d
e
f
FSC
Resolution (angstroms)
FSC
Resolution (angstroms)

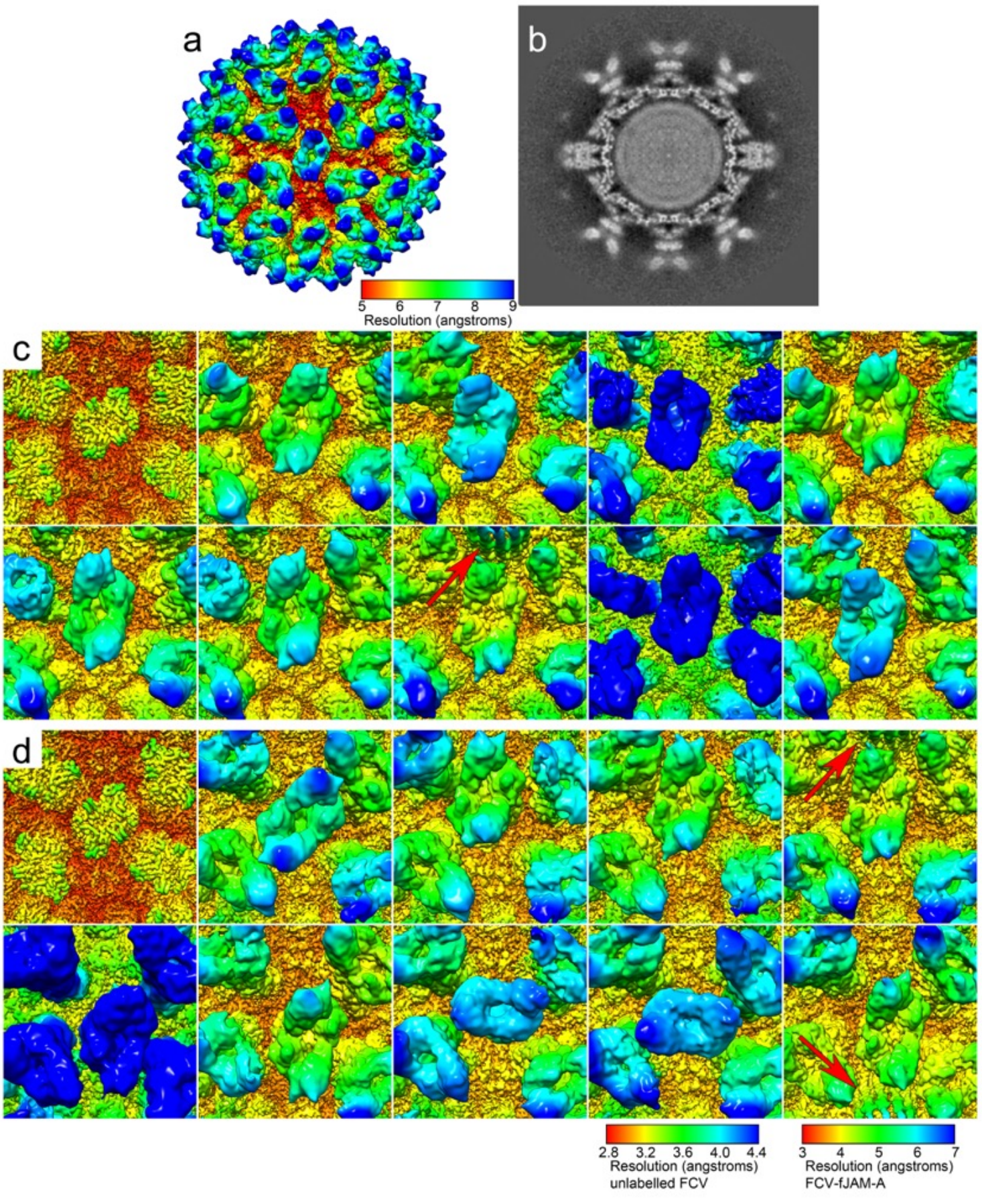
a
b
5 6 7 8 9
Resolution (angstroms)
c
d
2.8 3.2 3.6 4.0 4.4
Resolution (angstroms)
unlabelled FCV
3 4 5 6 7
Resolution (angstroms)
FCV-fJAM-A

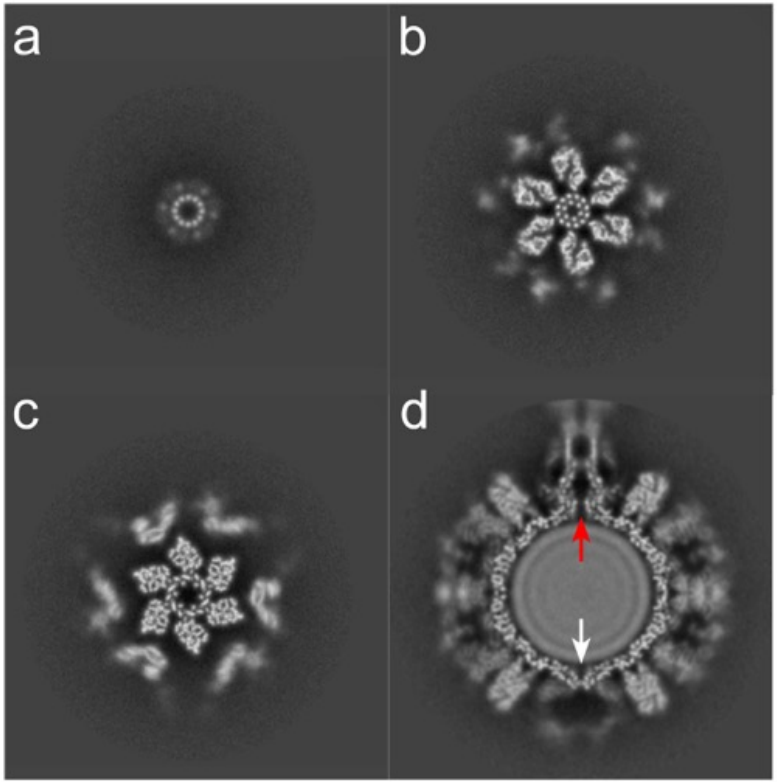
a
b
c
d

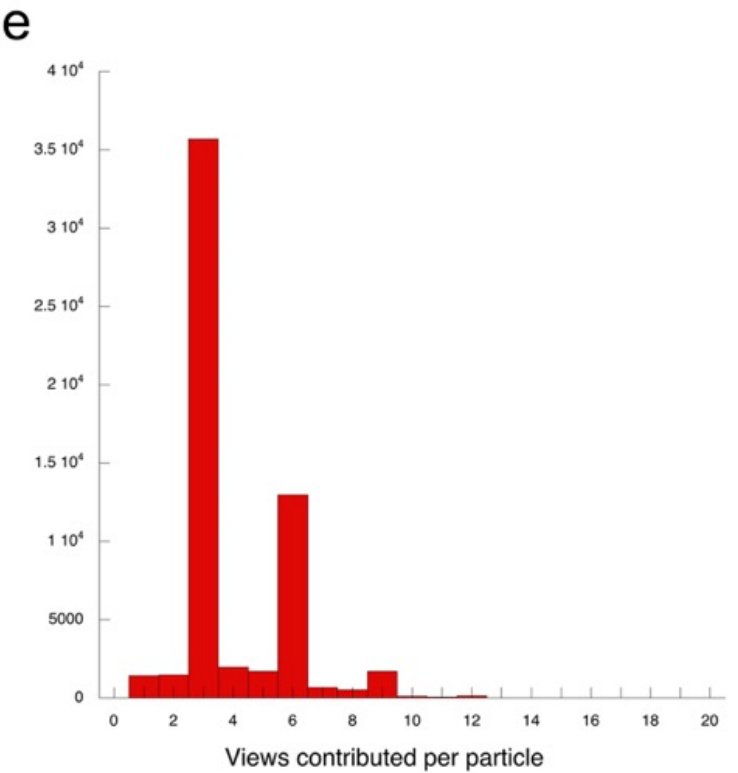
e
4 10⁴
3.5 10⁴
3 10⁴
2.5 10⁴
2 10⁴
1.5 10⁴
1 10⁴
5000
0
0
2
4
6
8
10
12
14
16
18
20
Views contributed per particle

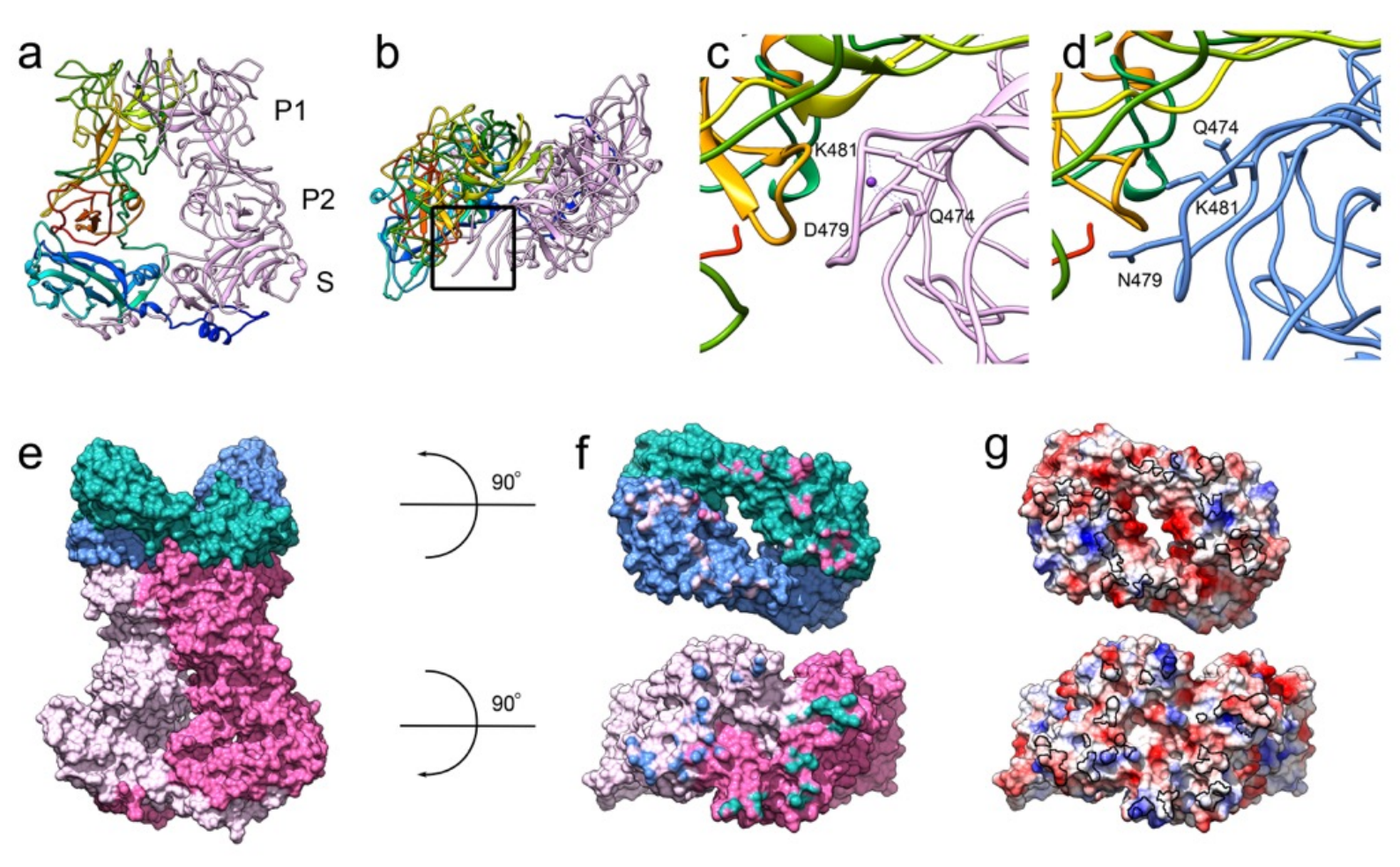
a
P1
P2
S
b
c
K481
D479
Q474
d
Q474
K481
N479
e
90°
90°
f
g

Cryo-EM data collection, refinement and validation statistics

	FCV VP1 (virion) (EMDB-0054) (PDB 6GSH)	FCV VP1, fJAM-A and VP2 (portal) (EMDB-0056) (PDB 6GSI)
Data collection and processing		
Magnification	75,000x	75,000x
Voltage (kV)	300	300
Electron exposure (e–/Å^2)	63	63
Defocus range (μm)	-1.2 to -3.5	-1.2 to -3.5
Pixel size (Å)	1.065	1.065
Symmetry imposed	I2	C3
Initial particle images (no.)	59,531	129,884
Final particle images (no.)	41,436	71,671
Map resolution (Å)	3	3.5
FSC threshold	0.143	0.143
Map resolution range (Å)	2.8-3.2	3.2-4.4
Refinement		
Initial model used (PDB code)	Undeposited homology model	PDB 6GSH
Model resolution (Å)		
FSC threshold		
Model resolution range (Å)		
Map sharpening *B* factor (Å^2)	-194	-182
Model composition		
Non-hydrogen atoms	12265	25390
Protein residues	12262	25386
Ligands	3	4
B factors (Å^2)		
Protein	mean = 32.7	mean = 118.0
Ligand	max = 84.9	max = 205.7
	min = 12.1	min = 67.5
	mean = 30.5	mean = 110.0
	max = 35.0	max = 123.7
	min = 25.6	min = 98.7
R.m.s. deviations		
Bond lengths (Å)	0.0104	0.0109
Bond angles (°)	1.30	1.24
Validation		
MolProbity score	1.66	2.08
Clashscore	3.33	7.47
Poor rotamers (%)	0.44 %	0.53 %
Ramachandran plot		
Favored (%)	90.63 %	84.60 %
Allowed (%)	9.05 %	15.22 %
Disallowed (%)	0.31 %	0.18 %

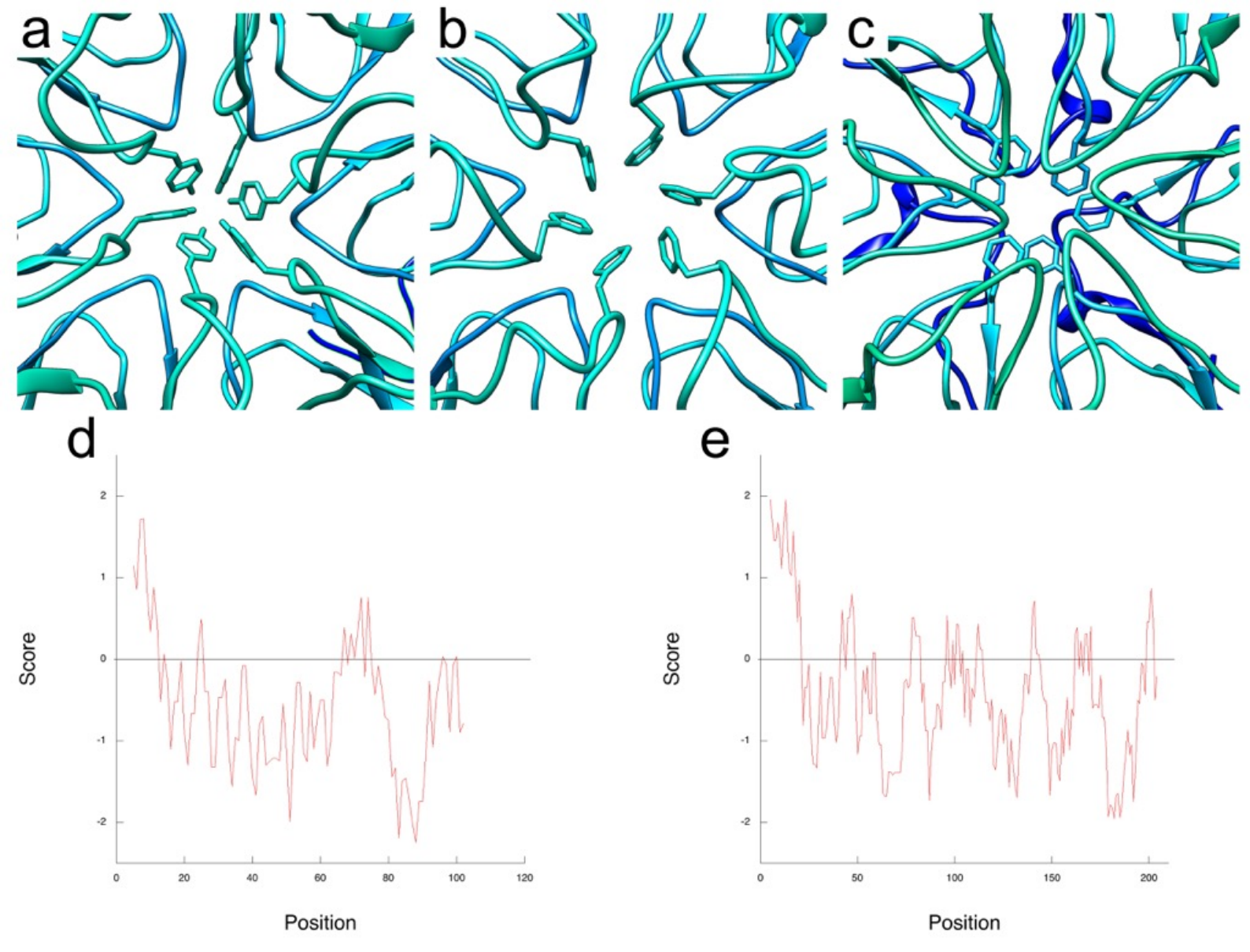
a
b
c
d
Score
2
1
0
-1
-2
0
20
40
60
80
100
120
Position
e
Score
2
1
0
-1
-2
0
50
100
150
200
Position

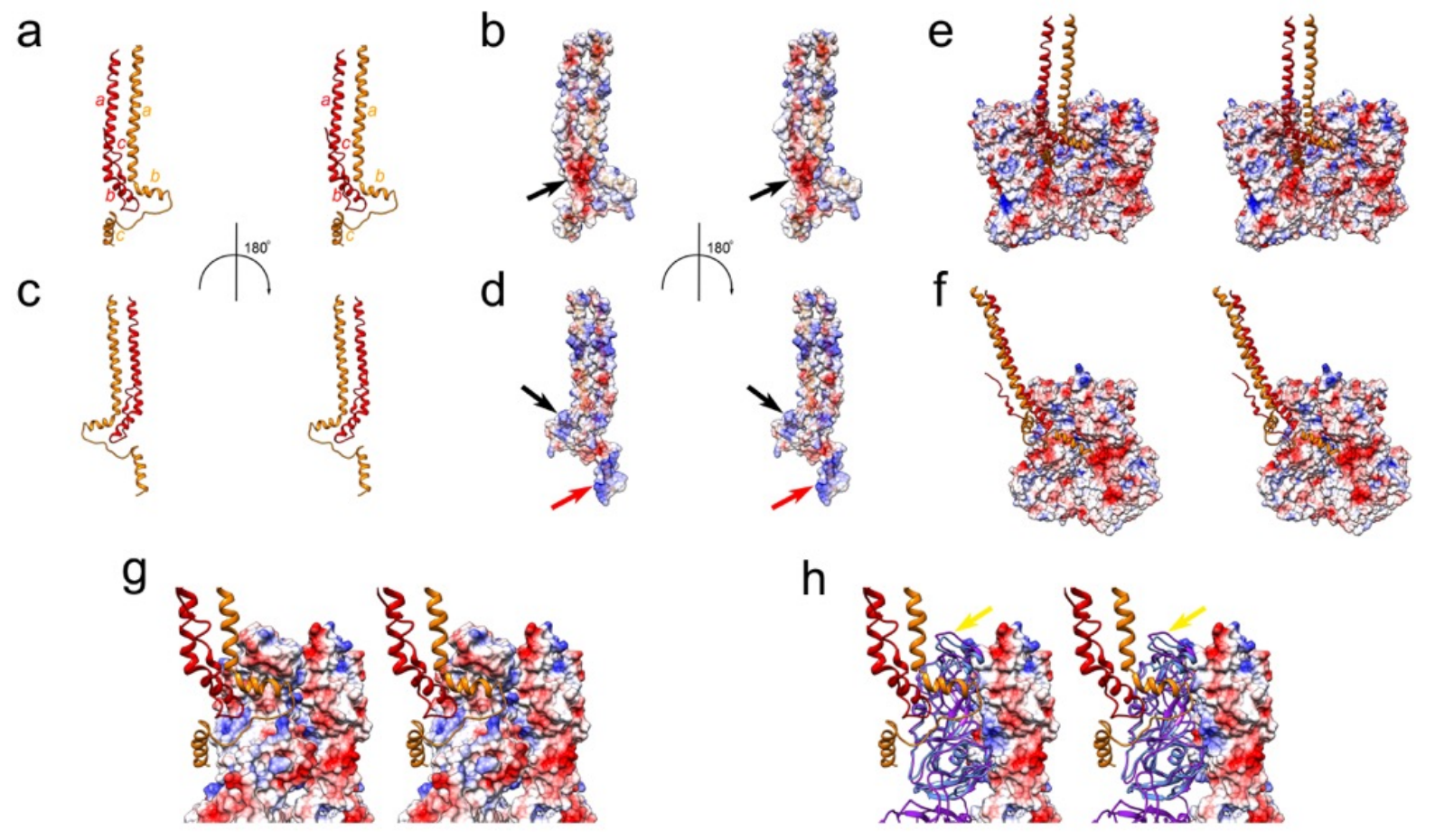
a
b
c
d
e
f
g
h
a
a
c
b
b
c
180°
180°

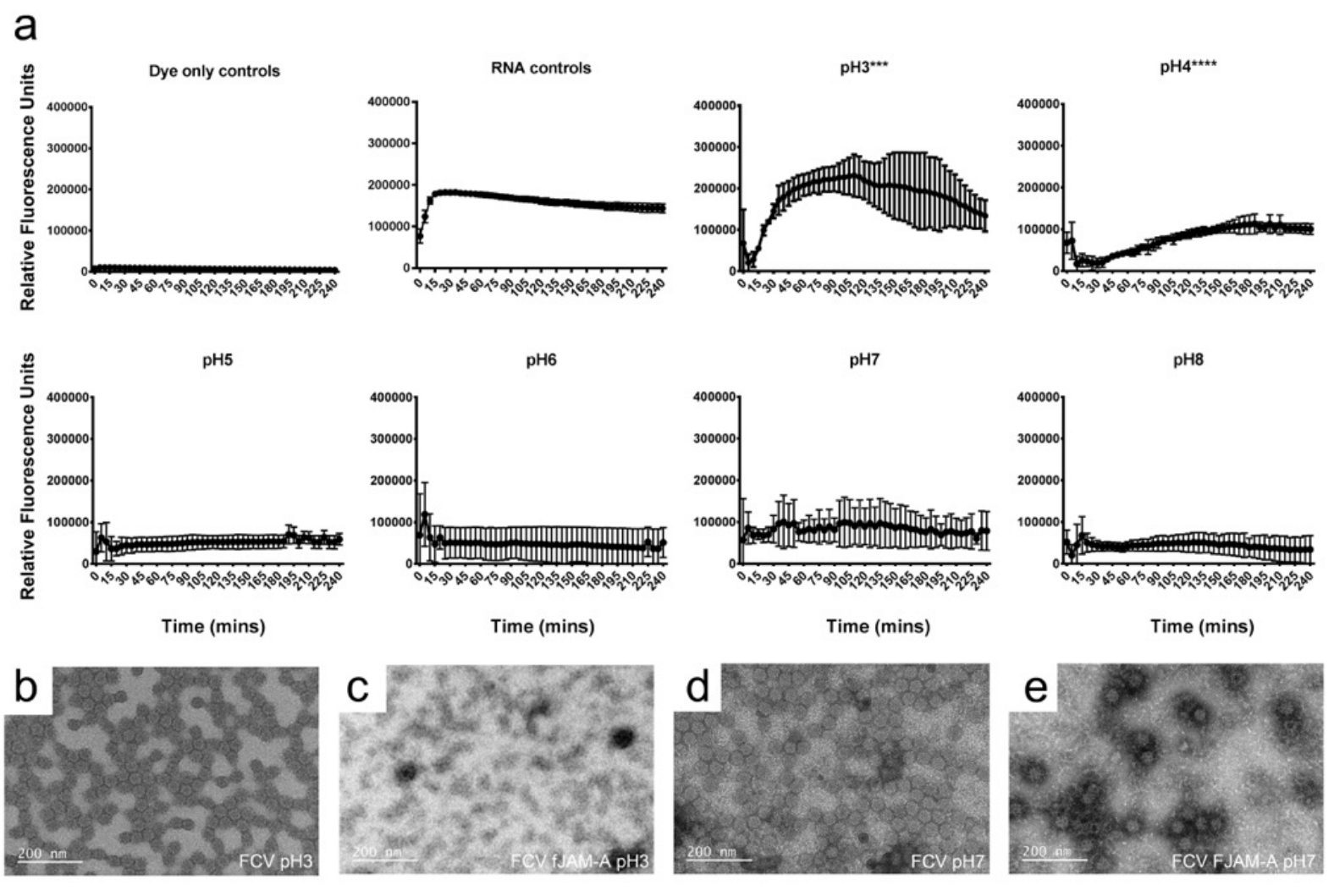
a
Dye only controls
RNA controls
pH3***
pH4****
pH5
pH6
pH7
pH8
Relative Fluorescence Units
Time (mins)
b
c
d
e
200 nm
FCV pH3
FCV fJAM-A pH3
FCV pH7
FCV FJAM-A pH7

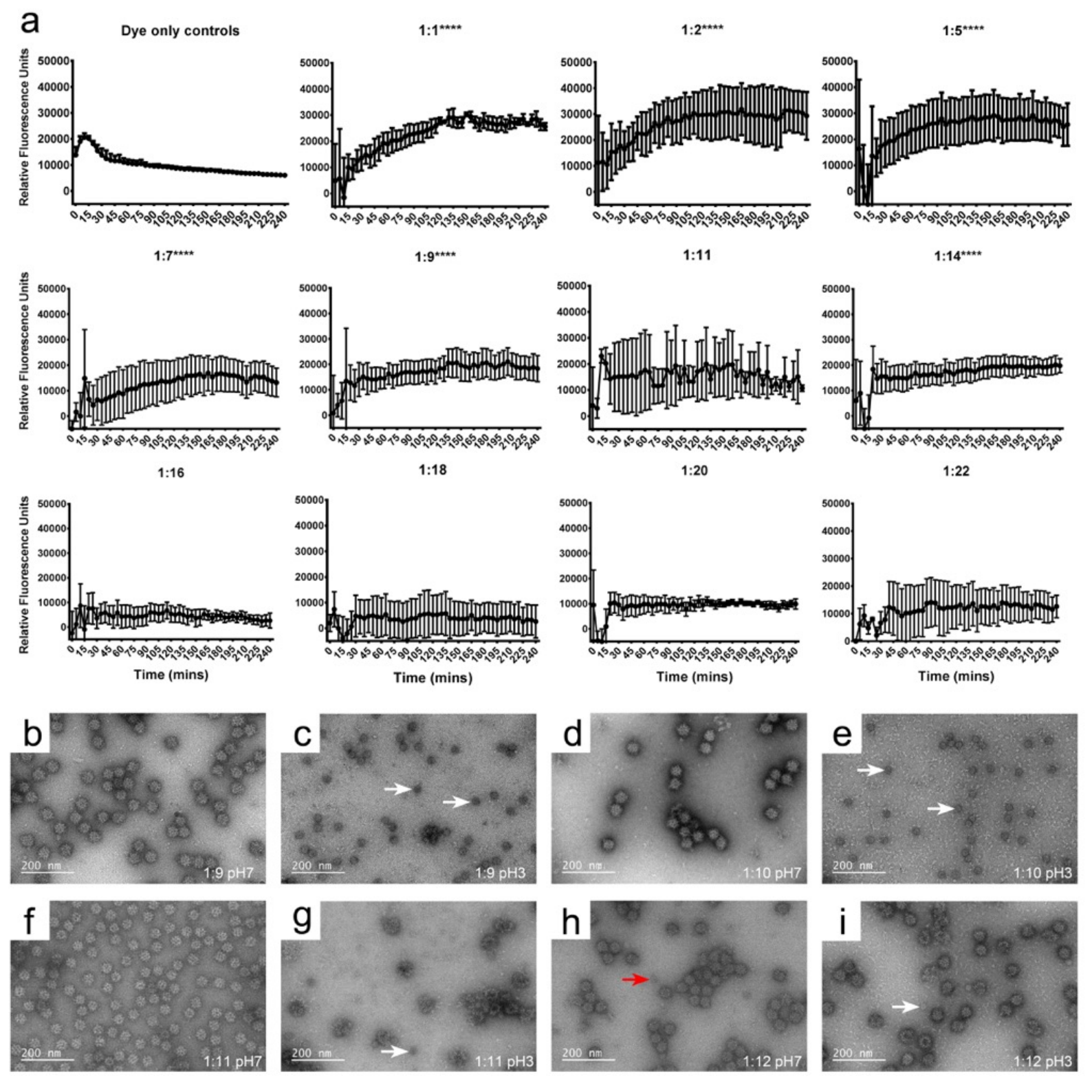
a
Dye only controls
1:1****
1:2****
1:5****
1:7****
1:9****
1:11
1:14****
1:16
1:18
1:20
1:22
Relative Fluorescence Units
Time (mins)
b
1:9 pH7
c
1:9 pH3
d
1:10 pH7
e
1:10 pH3
f
1:11 pH7
g
1:11 pH3
h
1:12 pH7
i
1:12 pH3
200 nm

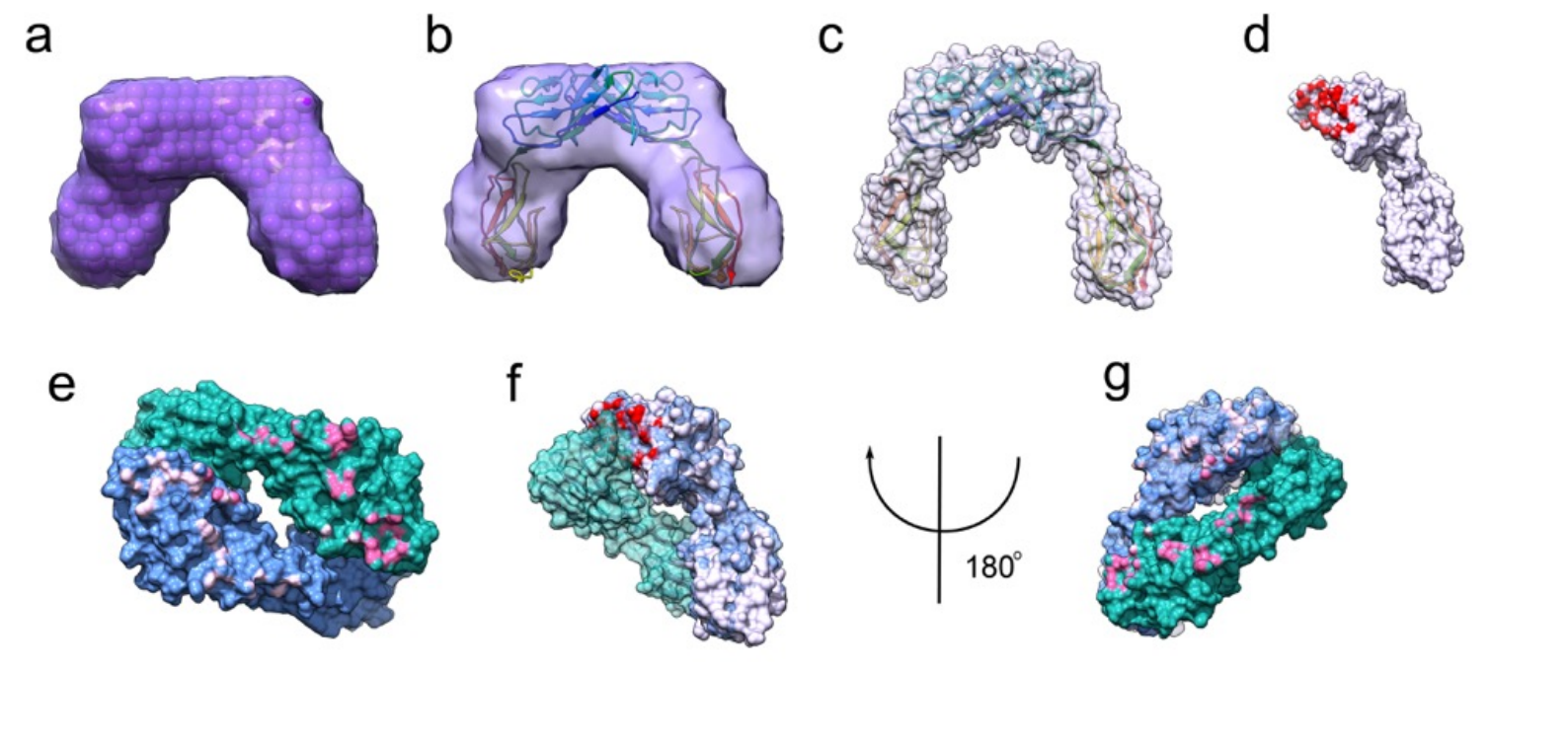
a
b
c
d
e
f
180°
g